

Q-SCHED: PUSHING THE BOUNDARIES OF FEW-STEP DIFFUSION MODELS WITH QUANTIZATION-AWARE SCHEDULING

000
001
002
003
004
005
006
007
008
009
010
011
012
013
014
015
016
017
018
019
020
021
022
023
024
025
026
027
028
029
030
031
032
033
034
035
036
037
038
039
040
041
042
043
044
045
046
047
048
049
050
051
052
053
Anonymous authors
Paper under double-blind review

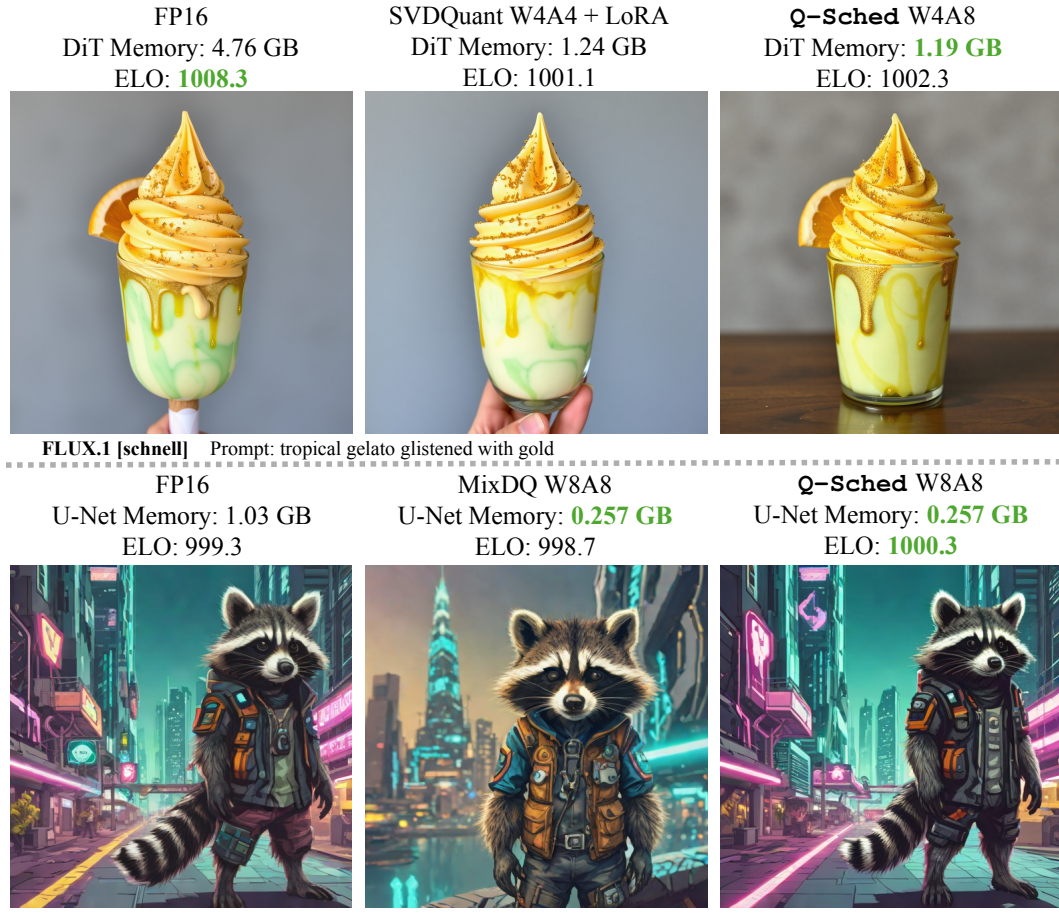


Figure 1: When large diffusion models are reduced to W8A8 or W4A8 for deployment, image fidelity drops. Q-Sched applies scheduler-level tuning, just two coefficients per step, to steer the sampler back to FP16-like quality, with no new checkpoints, no finetuning, and no extra FLOPs.

ABSTRACT

Text-to-image diffusion models remain computationally intensive: generating a single image typically requires dozens of passes through large transformer backbones (e.g., SDXL uses ~ 50 evaluations of a 2.6B-parameter model). Few-step variants reduce the step count to 2–8, but still rely on large, full-precision U-Net/DiT backbones, making inference impractical on resource-constrained platforms, both on-device (latency/energy) and in data centers with multi-instance GPU (MIG) style GPU partitioning (limited memory/throughput per slice). Existing post-training quantization (PTQ) methods are further hampered by dependence on full-precision calibration.

We introduce Q-Sched, a scheduler-level PTQ approach that adapts the diffusion sampler rather than the model weights. By adjusting the few-step sampling tra-

054
 055
 056
 057
 058
 059
 060
 jectory with quantization-aware preconditioning coefficients, Q-Sched matches
 or surpasses full-precision quality while delivering a $4\times$ reduction in model size
 and preserving a single reusable checkpoint across bit-widths. To learn these
 coefficients, we propose a reference-free Joint Alignment–Quality (JAQ) loss,
 which combines text–image compatibility with an image-quality objective for fine-
 grained control; JAQ requires only a handful of calibration prompts and avoids any
 full-precision inference during calibration.

061
 062
 063
 064
 065
 Empirically, Q-Sched yields substantial gains: a **15.5% FID improvement** over
 the FP16 4-step Latent Consistency Model and a **16.6% improvement** over the FP16
 8-step Phased Consistency Model, demonstrating that quantization and few-step
 distillation are complementary for high-fidelity generation. A large-scale user study
 with **80,000+** annotations further validates these results on both FLUX.1[schnell]
 and SDXL-Turbo. Code will be released.

068 1 INTRODUCTION 069

070 Diffusion models have achieved state-of-the-art generative quality across vision (Amit et al., 2021;
 071 Baranchuk et al., 2021; Brempong et al., 2022; Ho et al., 2022; Meng et al., 2021; Yang et al., 2022a),
 072 language (Austin et al., 2021; Li et al., 2022b), multimodal modeling (Avrahami et al., 2022; Ramesh
 073 et al., 2022), and scientific domains (Anand & Achim, 2022; Cao et al., 2022). Yet systems such
 074 as Stable Diffusion XL (Podell et al., 2023; Meng et al., 2021) and CogVideoX (Yang et al., 2024)
 075 remain costly at inference time: denoising typically requires tens to hundreds of steps, each invoking
 076 a large U-Net or Diffusion transformer (DiT) (Peebles & Xie, 2023).

077 Practical deployment therefore hinges on two levers: (1) reducing the number of function evaluations
 078 (few-step sampling), and (2) lowering the cost per evaluation (compression via quantization (He
 079 et al., 2024; Guo et al., 2022), pruning (Fang et al., 2024), or distillation (Huang et al., 2024)). These
 080 levers are particularly important in two widely used settings. *On-device*, memory and compute
 081 budgets are tight, latency and energy constraints are strict, and privacy/offline use cases preclude
 082 server offloading (Zhao et al., 2024b). *In data centers with MIG partitioning*, a single GPU is sliced
 083 into multiple smaller instances to increase concurrency and predictability; each slice has limited
 084 memory/throughput, making model footprint and per-step cost decisive (Zhang et al., 2023; Li et al.,
 085 2022a). In both cases, few-step sampling and quantization are natural, complementary choices.

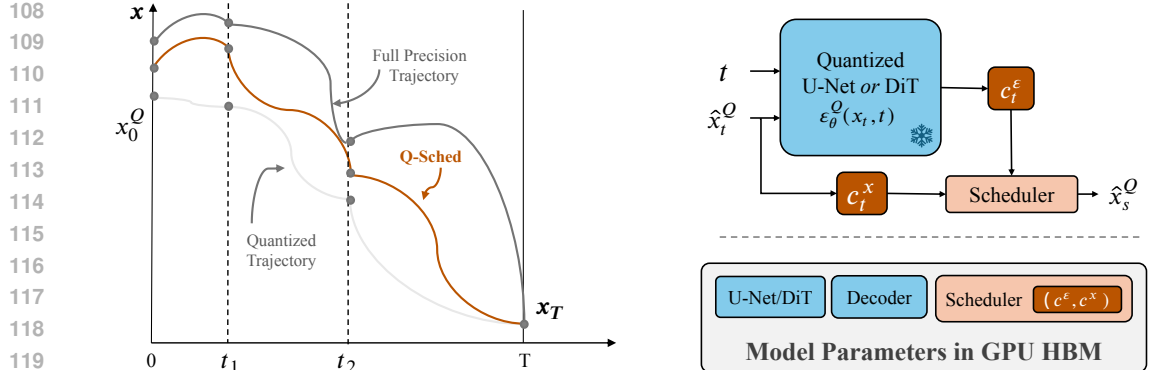
086 However, few-step acceleration is sensitive to the accuracy of the underlying probability-flow ordinary
 087 differential equation (ODE) or variance-preserving stochastic differential equation (SDE) that links
 088 the noise-estimation network to the final sample (Song et al., 2021). Quantization perturbs that
 089 network, inducing a mismatch that alters the ODE/SDE trajectory and amplifies artifacts, an effect
 090 that becomes more pronounced as the number of steps shrinks. Simply reusing full-precision
 091 schedulers on quantized backbones will inevitably induce quality degradation.

092 To bridge this gap, we introduce **Q-Sched**, a quantization-aware noise scheduler that adapts the
 093 few-step trajectory to the compressed model *without modifying any weights*. Q-Sched inserts
 094 lightweight coefficients (c^x, c^e) into the scheduler (Figures 2a and 2b), correcting quantization-
 095 induced drift while keeping a single U-Net/DiT checkpoint reusable across FP16, W8A8, and W4A8
 096 deployments. This design directly targets the constraints above: it preserves the latency benefits of
 097 few-step sampling, fits within on-device and MIG memory budgets, and avoids checkpoint sprawl in
 098 production.

099 Our contributions are summarized as follows:

100

- 101 1. In this work, we introduce **Q-Sched**, a quantization-aware scheduler that integrates seam-
 102 lessly with few-step diffusion models. It achieves up to a **15.5% FID improvement** over a
 103 4-step latent consistency model (LCM) (Luo et al., 2023) baseline and, as shown in Figure 1,
 104 can match or surpass full-precision arena scores *while simultaneously reducing model size*
 105 on SDXL-Turbo (4-Step) (Sauer et al., 2024) and FLUX.1[schnell] (Black Forest Labs,
 106 2024).
- 107 2. Q-Sched’s novel **preconditioning coefficients** enable quantized models to deliberately
 deviate from potentially overfit few-step baselines (Figure 2a), alleviating oversmoothing



108
109
110
111
112
113
114
115
116
117
118
119
120
121
122
123
124
125
126
127
128
129
130
131
132
133
134
135
136
137
138
139
140
141
142
143
144
145
146
147
148
149
150
151
152
153
154
155
156
157
158
159
160
161

(a) Quantization shifts the diffusion sampling trajectory, reducing fidelity. Q-Sched corrects this drift by adapting the scheduler.
(b) At timestep $t \rightarrow s$, Q-Sched applies lightweight coefficients (c_t^x, c_t^e) within the scheduler, enabling deployment of quantized models from a single U-Net/DiT checkpoint.

Figure 2: Q-Sched directly optimizes the few-step diffusion scheduler (see Figures 2a and 2b), addressing quantization-induced trajectory drift without modifying model weights. Unlike prior approaches that alter the transformer or U-Net backbone through retraining or post-training adjustments, Q-Sched leaves weights fixed, allowing seamless reuse of one pretrained checkpoint across FP16, W8A8, and W4A8 deployments. This simplifies model management and reduces storage overhead while maintaining high image fidelity.

and texture artifacts from distillation and quantization while improving the balance between fidelity and artifact severity.

3. To optimize these coefficients, we propose the **Joint Alignment–Quality (JAQ) loss** which balances perceptual fidelity with text–image alignment. Being reference-free, JAQ also enables precise control over visual properties (e.g., texture, detail, saturation) without requiring access to a full-precision model.
4. We establish a **theoretical existence guarantee** (Theorem 1), proving that Q-Sched coefficients always exist which reduce expected sampling error relative to the original quantized scheduler. This provides a principled explanation for Q-Sched’s systematic improvements.
5. Finally, a large-scale **human preference study** with over 80,000 annotations demonstrates that Q-Sched outperforms MixDQ (Zhao et al., 2024a) on SDXL-Turbo and SVDQuant (Li et al., 2025) on FLUX.1[schnell] in terms of perceived image quality.

As illustrated in Figure 1, Q-Sched attains the highest ELO rating in pairwise image-quality comparisons among evaluated methods. Furthermore, Figure 3 shows that Q-Sched is Pareto-optimal with respect to both ELO and model size, underscoring its ability to balance perceptual quality and efficiency more effectively than competing approaches.

2 BACKGROUND AND RELATED WORK

Diffusion models generate samples by denoising corrupted data across a trajectory of timesteps $t \in [0, T]$, where T is typically large (≥ 25). Each step applies a denoising network \mathcal{E}_θ , conditioned on both t and its noisy input x_t . While this iterative scheme yields high-fidelity samples, invoking a large U-Net or DiT backbone at every step makes inference prohibitively slow in deployment.

Recent few-step models highlight this bottleneck. **SDXL-Turbo** leverages Adversarial Diffusion Distillation (ADD), combining score distillation with an adversarial loss, to reduce sampling to just 1–4 steps, enabling real-time generation on commodity GPUs (Sauer et al., 2024). **FLUX.1[schnell]** introduces a 12B-parameter rectified-flow transformer with open weights, optimized for 1–4 step inference, making it attractive for latency-constrained serving (Black Forest Labs, 2024). Most recently, **FLUX.1[kontext]** extends the family beyond text-to-image toward *in-context* generation and

162 editing, accepting text and images jointly and unifying both tasks in a flow-matching framework (Labs
 163 et al., 2025). These advances exemplify the field’s shift toward *deployment-ready* diffusion systems
 164 that meet strict latency and memory budgets.

166 **Few-step diffusion and distillation.** Few-step methods compress the teacher’s long trajectory
 167 into a handful of evaluations, preserving most of the fidelity at a fraction of the cost. Distillation
 168 is the primary approach: early demonstrations distilled long-run teachers into 1–8 step students,
 169 such as Instaflow (Liu et al., 2023), rectified-flow straightening (Liu et al., 2022), and adversarially
 170 guided ADD (Sauer et al., 2024). Consistency Models (CMs) (Song et al., 2023) frame generation
 171 as a self-consistency mapping from any noisy state to the clean sample, yielding efficient few-
 172 step samplers. Variants include Latent Consistency Models (LCMs) (Luo et al., 2023) with Stable
 173 Diffusion (Rombach et al., 2022) backbones, Trajectory Consistency Distillation (TCD) (Zheng et al.,
 174 2024) with trajectory-aware schedules, and Phased Consistency Models (PCMs) (Wang et al., 2024)
 175 with improved guidance and stability. Across these designs, the *scheduler* plays a critical role in
 176 determining quality in the few-step regime. The update rule for few-step diffusion models using
 177 quantized backbone \mathcal{E}_θ^Q is:

$$x_s = \Phi(t, x_t, \mathcal{E}_\theta^Q), \quad (1)$$

180 where x_s denotes the intermediate sample at timestep $s \in [0, t]$ and $\Phi(\cdot)$ is a few-step scheduler.
 181 In Section 3, we illustrate our approach using the TCD scheduler (Zheng et al., 2024) as a running
 182 example. However, $Q\text{-Sched}$ is fully general and can be applied on top of any few-step scheduler
 183 that fits the abstraction in Equation (1).

184 **Quantization for diffusion models.** Post-training quantization (PTQ) has largely targeted \mathcal{E}_θ and its
 185 activations across timesteps. Timestep-aware calibration approaches (PTQ4DM (Shang et al., 2022),
 186 ADP-DM (Wang et al., 2023a), Q-Diffusion (Li et al., 2023)), dynamic schemes such as TDQ (So
 187 et al., 2024), and error-compensation methods (Q-DM (Li et al., 2024c)) all operate by modifying
 188 weights or activations and require full-precision calibration. MixDQ (Zhao et al., 2024a) extends to
 189 few-step models with a mixed-precision allocation strategy guided by begginning-of-sentence(BOS)-
 190 aware quantization and layer sensitivity analysis. SVDQuant (Li et al., 2025) targets 4-bit weights
 191 and activations by absorbing outliers into a high-precision low-rank branch via SVD, shifting variance
 192 from activations into weights before fusing the branch back into low-bit kernels.

193 We posit that in the few-step setting, quantization bias additionally manifests as a *scheduler mismatch*:
 194 a fixed full-precision schedule can systematically over- or under-correct, amplifying artifacts. One
 195 method that avoids modifying network weights is PTQD (He et al., 2024), which models the
 196 quantization-induced shift as an affine perturbation of the full-precision denoiser, $\mathcal{E}_\theta^Q(x_t, t) =$
 197 $(1 + \gamma)\mathcal{E}_\theta + \delta$, and compensates it via variance scaling and a bias term applied directly to the
 198 sampler update on x_t . In practice, γ is estimated via standard-deviation matching while δ is treated
 199 as uncorrelated Gaussian noise. We adapt PTQD-style bias correction, originally developed for
 200 *un-distilled* diffusion models, into TCD (see Section H) and generalize the principle to other few-step
 201 samplers as a baseline for our approach.

202 $Q\text{-Sched}$ reframes quantized few-step generation as scheduler adaptation. It learns quantization-
 203 aware preconditioning coefficients to correct trajectory drift with negligible overhead, while leaving
 204 the backbone frozen. The approach integrates seamlessly with few-step schedulers, needs only
 205 lightweight calibration, and preserves a single checkpoint across FP16, W8A8, and W4A8. Un-
 206 like prior PTQ methods that adjust weights or activations, $Q\text{-Sched}$ adapts the scheduler itself,
 207 complementing existing PTQ and distillation techniques to recover full-precision quality at reduced
 208 footprints while retaining the latency benefits of few-step sampling.

209 $Q\text{-Sched}$ differs fundamentally from prior bias and variance scaling methods like PTQD (He et al.,
 210 2024) by learning its correction coefficients end-to-end using final image quality, rather than relying
 211 on Gaussian assumptions or intermediate denoising states. By introducing a second coefficient
 212 on x_t and separating accumulated state error from current-step noise error, $Q\text{-Sched}$ gains the
 213 flexibility to correct both sources of distortion independently—crucial for few-step distilled models
 214 where intermediate distributions are no longer Gaussian. Overall, $Q\text{-Sched}$ removes dependency on
 215 full-precision activations, relaxes prior assumptions, and directly optimizes for the final output rather
 than intermediate signals.

216 **3 QUANTIZATION-AWARE SCHEDULING**
 217

218 To prepare the TCD scheduler for optimization with \mathcal{Q} -Sched, let us consider sampling with a
 219 quantized network. TCD’s Strategic Stochastic Sampling (SSS) (Zheng et al., 2024) using a quantized
 220 network $\mathcal{E}_\theta^Q(x_t, t)$ is given by:
 221

$$222 \quad \mathbf{x}_s = \frac{\alpha_s}{\alpha_{s'}} \left(\alpha_{s'} \frac{\mathbf{x}_t - \sigma_t \mathcal{E}_\theta^Q(x_t, t)}{\alpha_t} + \sigma_{s'} \mathcal{E}_\theta^Q(x_t, t) \right) + \eta \mathbf{z} \quad (2)$$

225 where the noise schedule is given by σ, α and the sampler injects stochastic noise sampled from a
 226 distribution $\mathbf{z} \sim N(0, I)$. The sampler relies on an intermediary timestep, $s' \in [s, t]$, where stochastic
 227 noise is added. The degree of randomness is controlled by the stochastic control parameter η :
 228

$$229 \quad \eta = \sqrt{1 - \frac{\alpha_s^2}{\alpha_{s'}^2}} \quad . \quad (3)$$

232 which can be adjusted at sampling time to vary image randomness. The TCD sampler in Equation (2),
 233 used in Phased Consistency Models, is a state-of-the-art few-step diffusion method that depends on
 234 two inputs from the previous step— x_t and $\mathcal{E}_\theta^Q(x_t, t)$ —which are central to applying \mathcal{Q} -Sched.
 235

236 **Q-Sched: A Learnable Schedule Pre-Conditioner** We introduce \mathcal{Q} -Sched, a lightweight post-
 237 training method that adapts the noise schedule of few-step diffusion models using two learnable
 238 scalar preconditioning coefficients, c_t^x and c_t^ϵ , applied respectively to x_t and $\mathcal{E}_\theta^Q(x_t, t)$ at time t .
 239 As illustrated in Figure 2b, \mathcal{Q} -Sched operates independently of the model backbone (U-Net or
 240 transformer), making it broadly compatible with any few-step scheduler resembling TCD.
 241

242 Under \mathcal{Q} -Sched, the TCD sampling update becomes:
 243

$$244 \quad \mathbf{x}_s = \frac{\alpha_s}{\alpha_{s'}} \left(\alpha_{s'} \frac{c_t^x \mathbf{x}_t - \sigma_t c_t^\epsilon \mathcal{E}_\theta^Q(x_t, t)}{\alpha_t} + \sigma_{s'} c_t^\epsilon \mathcal{E}_\theta^Q(x_t, t) \right) + \sqrt{1 - \frac{\alpha_s^2}{\alpha_{s'}^2}} \mathbf{z}. \quad (4)$$

247 In Equation (4), we explicitly show that \mathcal{Q} -Sched interacts with the update rule of common few-step
 248 scheduler. Because the update rule is affine in the preconditioning coefficients, $(\mathbf{c}^x, \mathbf{c}^\epsilon) := (c_t^x, c_t^\epsilon)_{t=0}^T$,
 249 they can be fused into the existing TCD coefficients without modifying the computational graph or
 250 adding inference cost. In the TCD formulation, the estimate at the proxy timestep s' is not obtained
 251 from a separate model evaluation but is derived directly from the prediction at timestep t . As a result,
 252 the noise term associated with s' inherits the same coefficient c_t^ϵ .
 253

253 To learn $(\mathbf{c}^x, \mathbf{c}^\epsilon)$, we perform hyperparameter search as outlined in Algorithm 1. While we describe
 254 the algorithm in terms of a generic optimizer, in practice, we find grid search is sufficient, as each
 255 model involves only two coefficients per timestep across 2–8 timesteps. In the grid search setting,
 256 `opt.step` simply advances to the next point in the predefined search grid. Even small adjustments
 257 to these coefficients yield noticeably crisper images with fewer quantization artifacts. More details
 258 about \mathcal{Q} -Sched’s search is in Section M.
 259

260 A natural question arises: **why are two coefficients sufficient to improve image quality?** It turns
 261 out that the reconstruction error between full precision and quantized images (at timestep $t = 0$),
 262 denoted by Δx_0 , can be strictly improved using scheduler coefficients:
 263

264 **Theorem 1** (Strict Existence Guarantees). *There exists \mathcal{Q} -Sched coefficients $(\mathbf{c}^x, \mathbf{c}^\epsilon) \neq 0$ such that
 $E[||\Delta \tilde{x}_0||] < E[||\Delta x_0||]$.*
 265

265 As shown in Appendix I, Δx_0 is a linear combination of per-step denoising errors $\Delta E_\theta(t)$ with
 266 coefficients k_t, m_t . Since the error is homogeneous in these terms, rescaling via $\tilde{k}_t = c_t^x k_t$ and
 267 $\tilde{m}_t = c_t^\epsilon m_t$ strictly reduces the expected error over naïve quantization. Thus, re-weighting the
 268 sampler, without modifying network weights, guarantees a reduction in error with respect to the full
 269 precision images. Next, we will discuss our new reference-free loss function, JAQ, and its advantages
 over existing image assessment tools.
 270

270

Algorithm 1 Search for Q-Sched Coefficients

271

272

273

274

275

276

277

278

279

280

281

282

283

284

285

286

287

288

289

290

291

292

Input: search range $[c_{min}, c_{max}]$, search points n , number of diffusion steps ω
loss function JAQ, calibration set \mathcal{C} , search optimizer opt

- 1: Initialize $S^* \leftarrow \infty$
- 2: \triangleright initialize each parameter in uniformly distributed range (c_{min}, c_{max})
- 3: $(c_{start}^x, c_{end}^x, c_{start}^\epsilon, c_{end}^\epsilon) \leftarrow \text{opt.init}(c_{min}, c_{max})$
- 4: **for** $i \in [0, n]$ **do**
- 5: $\mathbf{c}^x \leftarrow \text{linspace}(c_{start}^x, c_{end}^x, \omega)$
- 6: $\mathbf{c}^\epsilon \leftarrow \text{linspace}(c_{start}^\epsilon, c_{end}^\epsilon, \omega)$
- 7: $S \leftarrow []$
- 8: **for** $x \in \mathcal{C}$ **do**
- 9: $S_x \leftarrow \text{JAQ}(x; \mathbf{c}^x, \mathbf{c}^\epsilon)$
- 10: $S = S \cup S_x$
- 11: **end for**
- 12: $\triangleright \bar{S}$ is the arithmetic mean of S
- 13: **if** $\bar{S} < S^*$ **then**
- 14: $S^* \leftarrow \bar{S}$, $\mathbf{c}_*^x \leftarrow \mathbf{c}^x$, $\mathbf{c}_*^\epsilon \leftarrow \mathbf{c}^\epsilon$
- 15: **end if**
- 16: $(c_{start}^x, c_{end}^x, c_{start}^\epsilon, c_{end}^\epsilon) \leftarrow \text{opt.step}(\bar{S})$
- 17: **end for**
- 18: **return** $\mathbf{c}_*^x, \mathbf{c}_*^\epsilon$

293

294

295

296

297

298

299

300

301

302

303

JAQ: A Joint Alignment Quality Loss Function Because full precision intermediate states are unstable targets due to quantization-induced structural and semantic drift, optimizing directly for downstream image quality provides a far more reliable objective than attempting to match the full precision trajectory. Reference-free metrics such as CLIPScore (Hessel et al., 2021) have become essential for quick evaluation of text-to-image generation models and unlike FID (Heusel et al., 2017), SSIM (Wang et al., 2004), and other *comparative* metrics, reference-free metrics do not rely on a ground truth reference image and therefore are very useful in this setting. When quantizing these generative models, the resultant images, \hat{x}_0^Q , are generated by an altered sampling trajectory as evidenced in Figure 8, where \hat{x}_0^Q is a different, sometimes cleaner image than those derived from the full precision backbone. In short, the quantized model’s sampling trajectory coarsely follows the full precision model yet generates sufficient differences that reference-based metrics do not capture the image’s detail.

304

305

306

307

308

309

310

311

312

313

$$\text{JAQ}(x) = \text{TC}(x) + k \cdot \text{IQ}(x) \quad (5)$$

314

315

316

317

Optimizing solely for text–image compatibility (e.g., CLIPScore) sacrifices visual detail and fails to capture quantization artifacts (Figures 7 and 9). Conversely, relying only on image quality can generate extraneous details. JAQ balances these objectives through a linear combination, with k controlling the tradeoff between prompt fidelity and image detail.

318

319

320

321

322

323

Applying Q-Sched to Full Precision Models? While it is theoretically possible that applying Q-Sched to a non-quantized model could yield some improvement, this is not the setting the method is designed for. A full precision model is best optimized directly through its original training objectives such as distillation and fine-tuning rather than through a post-training scheduler adjustment. Q-Sched specifically targets post training degradation introduced by quantization and is intended to correct the resulting drift in the sampling trajectory.

Table 1: Comparison of different schedulers on Phased Consistency Models and Latent Consistency Models using a Stable Diffusion v1-5 backbone. The original schedule is TCD (Zheng et al., 2024) for Phased Consistency Models and the Multi-step Consistency Sampling (Luo et al., 2023) for Latent Consistency Models. The FID and CLIPScore are calculated with respect to the COCO-30k dataset. NFEs stands for *number of function evaluations* referring to the number of passes through the network $\mathcal{E}_\theta^Q(x_t, t)$. We report latency in milliseconds on an RTX A6000 GPU.

NFEs	Precision	Schedule	Latency (ms)	PCMs		LCMs	
				FID	CLIPScore	FID	CLIPScore
2	FP16	Original	148	24.17	<u>25.489</u>	38.74	<u>25.155</u>
	W4A8	Original	136	28.70	25.343	40.93	24.886
	W4A8	PTQD	137	<u>23.33</u>	25.265	<u>37.59</u>	24.919
	W4A8	Q-Sched	136	22.24	25.543	32.50	25.152
4	FP16	Original	193	23.29	25.482	<u>31.94</u>	25.969
	W4A8	Original	172	23.08	25.557	38.41	<u>25.456</u>
	W4A8	PTQD	172	<u>19.42</u>	25.639	39.72	24.678
	W4A8	Q-Sched	172	17.39	25.715	26.98	25.336
8	FP16	Original	286	20.15	25.714	<u>27.34</u>	26.052
	W4A8	Original	245	18.48	25.664	<u>27.55</u>	<u>25.397</u>
	W4A8	PTQD	246	15.85	25.770	28.06	<u>25.241</u>
	W4A8	Q-Sched	245	<u>16.83</u>	25.698	25.82	25.214

4 EXPERIMENTS

Experimental Setup We apply Q-Sched across diverse few-step diffusion models, including U-Net (Ronneberger et al., 2015) and DiT (Peebles & Xie, 2023) backbones, and across different distillation strategies: consistency-based (LCM (Luo et al., 2023), PCM (Wang et al., 2024)) and flow-matching approaches (SDXL-Turbo (Sauer et al., 2024) and FLUX.1[schnell] (Black Forest Labs, 2024)). We quantize models in both 4-bit weights, 8-bit activations (W4A8) and 8-bit weights, 8-bit activations (W8A8). Only the U-Net or DiT backbone is quantized, as it dominates model size (see Table 5).

Latency is measured on an Nvidia RTX A6000 GPU with Ampere compute architecture. Using BitsandBytes bit (2025), we quantize each model to 4-bit weights, 8-bit activations and average latency over 10 runs with a 3-run warmup phase.

LCM and PCM are tested at 2, 4, and 8 steps on COCO-30k (Lin et al., 2014), using FID (vs. real), CLIPScore (prompt alignment), and FID-SD (vs. Stable Diffusion). FLUX.1 and SDXL-Turbo are evaluated on the SVDQuant (Li et al., 2025; 2024b) subset of MJHQ-30k (5,000 high-quality Midjourney prompts in 10 categories), using FID and human preference studies to capture perceptual quality.

We employ two variants of the Joint Alignment Quality (JAQ) loss: one derived from CLIP-based metrics and another from human preference scores. In the CLIP-based variant, we set $TC(x) = CLIPScore(x)$ and $IQ(x) = CLIP-IQA(x)$. For SDXL-Turbo and FLUX.1, we instead adopt a preference-based variant, with $TC(x) = AQ-MAP(x)$ and $IQ(x) = HPSV2(x)$. Here, AQ-MAP (Li et al., 2024a) provides a spatial alignment score, while HPSV2 (Wu et al., 2023) is fine-tuned on real human judgments. In both cases, we fix $k = 2$.

Results: Latent and Phased Consistency Models In Table 1, we evaluate three schedulers across two consistency model families and show that Q-Sched learns a new few-step trajectory that mitigates artifacts and can even surpass both FP16 and W4A8 in detail. It achieves strong FID scores and outperforms PTQD in 4/6 consistency variants on Stable Diffusion v1-5, while using only a fraction of the calibration set. We compare with PTQD (He et al., 2024), the only other quantization-aware scheduler for few-step diffusion. Unlike PTQD, which relies on a 1,024-image full-precision calibration set, Q-Sched requires only 20 representative sDCI prompts (Li et al., 2025), reused across evaluations. Calibration overfitting is a common issue in PTQ methods, but

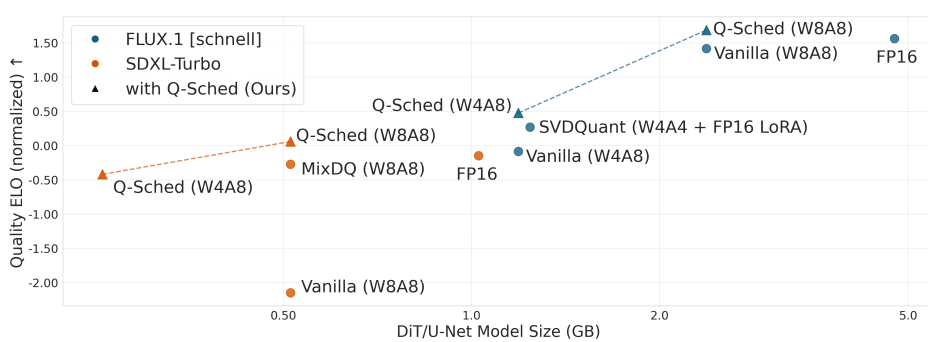


Figure 3: ELO Score vs. Model Size for various quantization methods on FLUX.1[schnell] (Black Forest Labs, 2024) and SDXL-Turbo (Sauer et al., 2024).

we mitigate it by using a highly descriptive long-form sDCI calibration set and optimizing only a small number of coefficients. This helps the quantized model learn to handle complex scenes, which generalizes well to simpler prompts. Our results show that this strategy yields strong performance on MJHQ and COCO-30k, two distinct downstream datasets. Unlike PTQD, which requires full-precision references, Q-Sched operates with just twenty prompts and can exceed a full precision few-step model by **16.1%, 15.5%, and 5.6%** at 2, 4, and 8 steps, respectively. This highlights that quantization and few-step distillation act as complementary compression strategies.

Furthermore, we would like to emphasize that Q-Sched and PTQD do not add any additional latency overhead to the sampler, since their coefficients can be fused to the existing schedule at inference time.

Scheduler	Precision	FID	FID-SD	CLIPScore
TCD	FP16	18.65	10.45	26.531
TCD	W4A8	22.70	12.51	26.241
PTQD	W4A8	161.96	176.29	25.910
Q-Sched	W4A8	18.89	12.17	26.513

(a) Comparison on a 2-step Phased Consistency model using the Stable Diffusion XL backbone. FID-SD is computed relative to images generated by Stable Diffusion XL using corresponding COCO-30k prompts.

Method	Precision	FID
-	FP16	25.48
Naive	W4A8	25.75
MixDQ	W4A8	25.36
Q-Sched	W4A8	21.41
Naive	W8A8	25.49
MixDQ	W8A8	25.16
Q-Sched	W8A8	26.34

(b) Quantized model comparison on SDXL-Turbo under varying bitwidths. FID is computed on the MJHQ dataset.

Table 2: Quantitative evaluation of Large-scale few-step diffusion models with a Stable Diffusion XL backbone. W4A8 and W8A8 are a $4\times$ and $8\times$ model size reduction in comparison to FP16, yet our method improves over baseline. As FID, FID-SD, and CLIPScore may exhibit reduced reliability at large model scales, we complement these metrics with user preference studies in Figure 3.

In Table 2a, we evaluate a large-scale 2-step Phased Consistency Model on the Stable Diffusion XL backbone. Q-Sched incurs only a 1.2% FID drop in W4A8, showing that quantization-aware preconditioning preserves quality even under aggressive compression. By contrast, PTQD degrades sharply, as its Gaussian noise assumption breaks down in few-step diffusion—particularly for large models where each step approximates an ODE segment rather than a Gaussian denoising step.

Results: SDXL-Turbo and FLUX.1[schnell] In Table 2b, we compare quantization strategies on SDXL-Turbo (4-step inference) using the FID metric on the MJHQ dataset, evaluating two bitwidth settings: W4A8 and W8A8. Under W4A8, Q-Sched achieves a FID of 21.41 with a standard deviation (std) of 0.15, significantly outperforming MixDQ (Zhao et al., 2024a) (25.36, std 0.17) and Naive (25.75, std 0.28), demonstrating strong robustness to aggressive quantization. Q-Sched

432 Table 3: Comparison across image quality metrics. "MixDQ" refers to the W8A8 MixDQ (Zhao
 433 et al., 2024a) variant and "SVDQ" refers to LoRA-based W4A4 SVDQuant Li et al. (2025).

	SDXL-Turbo (4-Step)				FLUX.1 [schnell]			
	FP16	W8A8	MixDQ	Q-Sched	FP16	W4A8	SVDQ	W4A8 Q-Sched
CLIP Score \uparrow	25.62	25.62	25.38	25.36	25.61	25.17	25.52	25.27
CLIP IQA \uparrow	0.725	0.727	0.727	0.731	0.716	0.712	0.714	0.707
HPV2 \uparrow	0.276	0.276	0.275	0.278	0.275	0.274	0.275	0.272
AQ-MAP \uparrow	0.693	0.694	0.693	0.696	0.700	0.700	0.697	0.700
Pick Score \uparrow	18.48	18.49	18.48	18.51	18.43	18.42	18.40	18.46
MANIQA \uparrow	0.508	0.513	0.502	0.511	0.528	0.500	0.514	0.506
JAQ (ours) \uparrow	1.663	1.665	1.659	1.669	1.676	1.675	1.669	1.673

444
 445 learns its own sampling trajectory—often improving image quality despite FID fluctuations—and
 446 across diverse metrics it remains competitive with, and sometimes better than, both state-of-the-art
 447 quantization methods and full-precision models. However, at W8A8, Q-Sched shows a higher
 448 FID (26.34) than both MixDQ (25.16) and Naive (25.49), suggesting that its advantages are most
 449 pronounced in lower-bit regimes, where other methods degrade more severely.

450 In Figure 3, we present user preference results for Q-Sched applied to both SDXL-Turbo and FLUX.1 [schnell], showing that
 451 it outperforms MixDQ (Zhao et al., 2024a) and SVDQuant (Li
 452 et al., 2025), respectively, at similar model sizes (see Section B
 453 for details). We compute an ELO rating, a relative quality rank-
 454 ing inspired by chess scoring, by aggregating all pairwise 1v1
 455 image comparisons across models, where a higher score reflects
 456 consistent user preference.

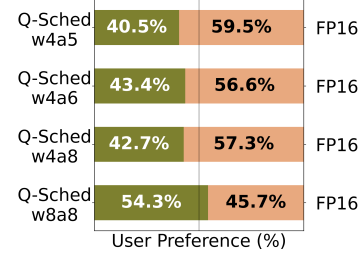
457 In Figure 4, we compare Q-Sched across bit-widths using a
 458 user study. W4A4 proved too aggressive, but W4A5 and W4A6
 459 produced images comparable to full precision. 1v1 comparisons
 460 with full-precision FLUX.1 (Black Forest Labs, 2024) follow
 461 the protocol in Appendix B.

462 Comparison with Image Quality Metrics We also evaluate

463 Q-Sched on FLUX.1[schnell] and SDXL-Turbo using human preference metrics, showing that
 464 JAQ effectively captures image fidelity. Beyond the metrics we've already mentioned, we compare
 465 with PickScore (Kirstain et al., 2023) which predicts human preferences from large-scale image–text
 466 comparisons, and MANIQA (Yang et al., 2022b) which uses multi-dimensional attention to assess
 467 perceptual quality without references. As seen in Table 3, JAQ aligns closely with established metrics
 468 while uniquely balancing fine-grained details often degraded by quantization.

469
 470 **Ablation on Pre-Conditioning Coefficients and Loss Function Choice** We ablate the choice of
 471 pre-conditioning coefficients in the Phased Consistency Model by comparing performance when
 472 optimizing only the model-side coefficient c^ϵ , the sample-side coefficient c^x , or both jointly. As
 473 shown in Figure 5b, jointly optimizing both c^ϵ and c^x consistently yields the best results across all
 474 three metrics: PickScore, HPSv2, and JAQ Loss. These findings highlight the importance of treating
 475 both denoising and reconstruction terms as tunable components rather than fixing one a priori. All
 476 metrics are averaged over 1024 images generated with the SDXL backbone.

477
 478 **How Do We Choose k For The JAQ Loss?** We optimize the Q-Sched preconditioners using the
 479 JAQ loss, which balances image quality and text-image consistency via a tradeoff hyperparameter, k .
 480 As shown in Figure 5a, small k values can lead to color distortion, while larger values (e.g., $k = 5$)
 481 cause outputs to drift from the true data distribution. In such cases, the JAQ loss behaves similarly to
 482 CLIP-IQA-Q, which lacks sensitivity to concept alignment. We find that a hand-tuned value of k is
 483 sufficient for producing a high-quality noise schedule, and the final results are not highly sensitive to
 484 its exact choice. Throughout our experiments, we use $k = 2$.



485 Figure 4: Comparing Q-Sched across various bit-widths.

540 Jacob Austin, Daniel D Johnson, Jonathan Ho, Daniel Tarlow, and Rianne van den Berg. Structured
 541 denoising diffusion models in discrete state-spaces. *Advances in Neural Information Processing*
 542 *Systems*, 34:17981–17993, 2021.

543

544 Omri Avrahami, Dani Lischinski, and Ohad Fried. Blended diffusion for text-driven editing of natural
 545 images. In *Proceedings of the IEEE/CVF Conference on Computer Vision and Pattern Recognition*,
 546 pp. 18208–18218, 2022.

547 Dmitry Baranchuk, Ivan Rubachev, Andrey Voynov, Valentin Khrulkov, and Artem Babenko. Label-
 548 efficient semantic segmentation with diffusion models. *arXiv preprint arXiv:2112.03126*, 2021.

549

550 Black Forest Labs. Flux.1-schnell. <https://huggingface.co/black-forest-labs/FLUX.1-schnell>, 2024. Accessed: 2025-05-14.

551

552 Emmanuel Asiedu Brempong, Simon Kornblith, Ting Chen, Niki Parmar, Matthias Minderer, and
 553 Mohammad Norouzi. Denoising pretraining for semantic segmentation. In *Proceedings of the*
 554 *IEEE/CVF Conference on Computer Vision and Pattern Recognition*, pp. 4175–4186, 2022.

555

556 Chentao Cao, Zhuo-Xu Cui, Shaonan Liu, Dong Liang, and Yanjie Zhu. High-frequency space
 557 diffusion models for accelerated mri. *arXiv preprint arXiv:2208.05481*, 2022.

558

559 Junsong Chen, Shuchen Xue, Yuyang Zhao, Jincheng Yu, Sayak Paul, Junyu Chen, Han Cai, Song
 560 Han, and Enze Xie. Sana-sprint: One-step diffusion with continuous-time consistency distillation.
 561 *arXiv preprint arXiv:2503.09641*, 2025.

562

563 Gongfan Fang, Xinyin Ma, and Xinchao Wang. Structural pruning for diffusion models. *Advances in*
 564 *neural information processing systems*, 36, 2024.

565

566 Cong Guo, Yuxian Qiu, Jingwen Leng, Xiaotian Gao, Chen Zhang, Yunxin Liu, Fan Yang, Yuhao
 567 Zhu, and Minyi Guo. Squant: On-the-fly data-free quantization via diagonal hessian approximation.
 568 *arXiv preprint arXiv:2202.07471*, 2022.

569

570 Yefei He, Luping Liu, Jing Liu, Weijia Wu, Hong Zhou, and Bohan Zhuang. Ptqd: Accurate post-
 571 training quantization for diffusion models. *Advances in Neural Information Processing Systems*,
 572 36, 2024.

573

574 Jack Hessel, Ari Holtzman, Maxwell Forbes, Ronan Le Bras, and Yejin Choi. Clipscore: A reference-
 575 free evaluation metric for image captioning. *arXiv preprint arXiv:2104.08718*, 2021.

576

577 Martin Heusel, Hubert Ramsauer, Thomas Unterthiner, Bernhard Nessler, and Sepp Hochreiter. Gans
 578 trained by a two time-scale update rule converge to a local nash equilibrium. *Advances in neural*
 579 *information processing systems*, 30, 2017.

580

581 Jonathan Ho, Chitwan Saharia, William Chan, David J Fleet, Mohammad Norouzi, and Tim Salimans.
 582 Cascaded diffusion models for high fidelity image generation. *J. Mach. Learn. Res.*, 23(47):1–33,
 583 2022.

584

585 Tao Huang, Yuan Zhang, Mingkai Zheng, Shan You, Fei Wang, Chen Qian, and Chang Xu. Knowl-
 586 edge diffusion for distillation. *Advances in Neural Information Processing Systems*, 36, 2024.

587

588 Yuval Kirstain, Adam Polyak, Uriel Singer, Shahbuland Matiana, Joe Penna, and Omer Levy. Pick-
 589 a-pic: An open dataset of user preferences for text-to-image generation. *Advances in neural*
 590 *information processing systems*, 36:36652–36663, 2023.

591

592 Black Forest Labs, Stephen Batifol, Andreas Blattmann, Frederic Boesel, Saksham Consul, Cyril
 593 Diagne, Tim Dockhorn, Jack English, Zion English, Patrick Esser, Sumith Kulal, Kyle Lacey, Yam
 594 Levi, Cheng Li, Dominik Lorenz, Jonas Müller, Dustin Podell, Robin Rombach, Harry Saini, Axel
 595 Sauer, and Luke Smith. Flux.1 kontext: Flow matching for in-context image generation and editing
 596 in latent space, 2025. URL <https://arxiv.org/abs/2506.15742>.

597

598 Baolin Li, Tirthak Patel, Siddharth Samsi, Vijay Gadepally, and Devesh Tiwari. Miso: exploiting
 599 multi-instance gpu capability on multi-tenant gpu clusters. In *Proceedings of the 13th Symposium*
 600 *on Cloud Computing*, pp. 173–189, 2022a.

594 Chunyi Li, Haoning Wu, Zicheng Zhang, Hongkun Hao, Kaiwei Zhang, Lei Bai, Xiaohong Liu,
 595 Xiongkuo Min, Weisi Lin, and Guangtao Zhai. Q-refine: A perceptual quality refiner for ai-
 596 generated image. In *2024 IEEE International Conference on Multimedia and Expo (ICME)*, pp.
 597 1–6. IEEE, 2024a.

598 Daiqing Li, Aleks Kamko, Ehsan Akhgari, Ali Sabet, Linmiao Xu, and Suhail Doshi. Playground
 599 v2.5: Three insights towards enhancing aesthetic quality in text-to-image generation, 2024b.

601 Muyang Li, Yujun Lin, Zhekai Zhang, Tianle Cai, Junxian Guo, Xiuyu Li, Enze Xie, Chenlin Meng,
 602 Jun-Yan Zhu, and Song Han. Svdquant: Absorbing outliers by low-rank component for 4-bit
 603 diffusion models. In *The Thirteenth International Conference on Learning Representations*, 2025.

604 Xiang Li, John Thickstun, Ishaan Gulrajani, Percy S Liang, and Tatsunori B Hashimoto. Diffusion-Im
 605 improves controllable text generation. *Advances in Neural Information Processing Systems*, 35:
 606 4328–4343, 2022b.

608 Xiuyu Li, Long Lian, Yijiang Liu, Huanrui Yang, Zhen Dong, Daniel Kang, Shanghang Zhang, and
 609 Kurt Keutzer. Q-diffusion: Quantizing diffusion models. *arXiv preprint arXiv:2302.04304*, 2023.

611 Yanjing Li, Sheng Xu, Xianbin Cao, Xiao Sun, and Baochang Zhang. Q-dm: An efficient low-bit
 612 quantized diffusion model. *Advances in Neural Information Processing Systems*, 36, 2024c.

613 Tsung-Yi Lin, Michael Maire, Serge Belongie, James Hays, Pietro Perona, Deva Ramanan, Piotr
 614 Dollár, and C Lawrence Zitnick. Microsoft coco: Common objects in context. In *Computer Vision-
 615 ECCV 2014: 13th European Conference, Zurich, Switzerland, September 6-12, 2014, Proceedings,
 616 Part V 13*, pp. 740–755. Springer, 2014.

617 Xingchao Liu, Chengyue Gong, and Qiang Liu. Flow straight and fast: Learning to generate and
 618 transfer data with rectified flow. *arXiv preprint arXiv:2209.03003*, 2022.

620 Xingchao Liu, Xiwen Zhang, Jianzhu Ma, Jian Peng, et al. Instaflow: One step is enough for
 621 high-quality diffusion-based text-to-image generation. In *The Twelfth International Conference on
 622 Learning Representations*, 2023.

624 Simian Luo, Yiqin Tan, Longbo Huang, Jian Li, and Hang Zhao. Latent consistency models:
 625 Synthesizing high-resolution images with few-step inference. *arXiv preprint arXiv:2310.04378*,
 626 2023.

627 Chenlin Meng, Yutong He, Yang Song, Jiaming Song, Jiajun Wu, Jun-Yan Zhu, and Stefano Ermon.
 628 Sdedit: Guided image synthesis and editing with stochastic differential equations. In *International
 629 Conference on Learning Representations*, 2021.

631 Anish Mittal, Anush Krishna Moorthy, and Alan Conrad Bovik. No-reference image quality as-
 632 sessment in the spatial domain. *IEEE Transactions on image processing*, 21(12):4695–4708,
 633 2012.

634 William Peebles and Saining Xie. Scalable diffusion models with transformers. In *Proceedings of
 635 the IEEE/CVF international conference on computer vision*, pp. 4195–4205, 2023.

637 Dustin Podell, Zion English, Kyle Lacey, Andreas Blattmann, Tim Dockhorn, Jonas Müller, Joe
 638 Penna, and Robin Rombach. Sdxl: Improving latent diffusion models for high-resolution image
 639 synthesis. *arXiv preprint arXiv:2307.01952*, 2023.

640 Aditya Ramesh, Prafulla Dhariwal, Alex Nichol, Casey Chu, and Mark Chen. Hierarchical text-
 641 conditional image generation with clip latents. *arXiv preprint arXiv:2204.06125*, 2022.

643 Rapidata. Rapidata: An api that provides fast access to large-scale human evaluations, 2025. URL
 644 <https://www.rapidata.ai/>. Accessed: 2025-05-16.

646 Robin Rombach, Andreas Blattmann, Dominik Lorenz, Patrick Esser, and Björn Ommer. High-
 647 resolution image synthesis with latent diffusion models. In *Proceedings of the IEEE/CVF Confer-
 ence on Computer Vision and Pattern Recognition*, pp. 10684–10695, 2022.

648 Olaf Ronneberger, Philipp Fischer, and Thomas Brox. U-net: Convolutional networks for biomedical
 649 image segmentation. In *Medical image computing and computer-assisted intervention—MICCAI*
 650 *2015: 18th international conference, Munich, Germany, October 5-9, 2015, proceedings, part III*
 651 18, pp. 234–241. Springer, 2015.

652 Axel Sauer, Dominik Lorenz, Andreas Blattmann, and Robin Rombach. Adversarial diffusion
 653 distillation. In *European Conference on Computer Vision*, pp. 87–103. Springer, 2024.

654 Yuzhang Shang, Zhihang Yuan, Bin Xie, Bingzhe Wu, and Yan Yan. Post-training quantization on
 655 diffusion models. *arXiv preprint arXiv:2211.15736*, 2022.

656 Junhyuk So, Jungwon Lee, Daehyun Ahn, Hyungjun Kim, and Eunhyeok Park. Temporal dynamic
 657 quantization for diffusion models. *Advances in Neural Information Processing Systems*, 36, 2024.

658 Yang Song, Jascha Sohl-Dickstein, Diederik P. Kingma, Abhishek Kumar, Stefano Ermon, and Ben
 659 Poole. Score-based generative modeling through stochastic differential equations, 2021.

660 Yang Song, Prafulla Dhariwal, Mark Chen, and Ilya Sutskever. Consistency models. *arXiv preprint*
 661 *arXiv:2303.01469*, 2023.

662 Changyuan Wang, Ziwei Wang, Xiuwei Xu, Yansong Tang, Jie Zhou, and Jiwen Lu. Towards accurate
 663 data-free quantization for diffusion models. *arXiv preprint arXiv:2305.18723*, 2(5), 2023a.

664 Fu-Yun Wang, Zhaoyang Huang, Alexander William Bergman, Dazhong Shen, Peng Gao, Michael
 665 Lingelbach, Keqiang Sun, Weikang Bian, Guanglu Song, Yu Liu, et al. Phased consistency model.
 666 *arXiv preprint arXiv:2405.18407*, 2024.

667 Jianyi Wang, Kelvin CK Chan, and Chen Change Loy. Exploring clip for assessing the look and
 668 feel of images. In *Proceedings of the AAAI Conference on Artificial Intelligence*, volume 37, pp.
 669 2555–2563, 2023b.

670 Zhou Wang, Alan C Bovik, Hamid R Sheikh, and Eero P Simoncelli. Image quality assessment: from
 671 error visibility to structural similarity. *IEEE transactions on image processing*, 13(4):600–612,
 672 2004.

673 Xiaoshi Wu, Yiming Hao, Keqiang Sun, Yixiong Chen, Feng Zhu, Rui Zhao, and Hongsheng Li.
 674 Human preference score v2: A solid benchmark for evaluating human preferences of text-to-image
 675 synthesis. *CoRR*, 2023.

676 Ruihan Yang, Prakhar Srivastava, and Stephan Mandt. Diffusion probabilistic modeling for video
 677 generation. *arXiv preprint arXiv:2203.09481*, 2022a.

678 Sidi Yang, Tianhe Wu, Shuwei Shi, Shanshan Lao, Yuan Gong, Mingdeng Cao, Jiahao Wang, and
 679 Yujiu Yang. Maniq: Multi-dimension attention network for no-reference image quality assessment.
 680 In *Proceedings of the IEEE/CVF conference on computer vision and pattern recognition*, pp. 1191–
 681 1200, 2022b.

682 Zhuoyi Yang, Jiayan Teng, Wendi Zheng, Ming Ding, Shiyu Huang, Jiazheng Xu, Yuanming Yang,
 683 Wenyi Hong, Xiaohan Zhang, Guanyu Feng, et al. Cogvideox: Text-to-video diffusion models
 684 with an expert transformer. *arXiv preprint arXiv:2408.06072*, 2024.

685 Huaizheng Zhang, Yuanming Li, Wencong Xiao, Yizheng Huang, Xing Di, Jianxiong Yin, Simon
 686 See, Yong Luo, Chiew Tong Lau, and Yang You. Migperf: A comprehensive benchmark for deep
 687 learning training and inference workloads on multi-instance gpus. *arXiv preprint arXiv:2301.00407*,
 688 2023.

689 Tianchen Zhao, Xuefei Ning, Tongcheng Fang, Enshu Liu, Guyue Huang, Zinan Lin, Shengen Yan,
 690 Guohao Dai, and Yu Wang. Mixdq: Memory-efficient few-step text-to-image diffusion models
 691 with metric-decoupled mixed precision quantization. In *European Conference on Computer Vision*,
 692 pp. 285–302. Springer, 2024a.

693 Yang Zhao, Yanwu Xu, Zhisheng Xiao, Haolin Jia, and Tingbo Hou. Mobiledonfusion: Instant
 694 text-to-image generation on mobile devices. In *European Conference on Computer Vision*, pp.
 695 225–242. Springer, 2024b.

702 Jianbin Zheng, Minghui Hu, Zhongyi Fan, Chaoyue Wang, Changxing Ding, Dacheng Tao, and
703 Tat-Jen Cham. Trajectory consistency distillation. *arXiv preprint arXiv:2402.19159*, 2024.
704
705
706
707
708
709
710
711
712
713
714
715
716
717
718
719
720
721
722
723
724
725
726
727
728
729
730
731
732
733
734
735
736
737
738
739
740
741
742
743
744
745
746
747
748
749
750
751
752
753
754
755